


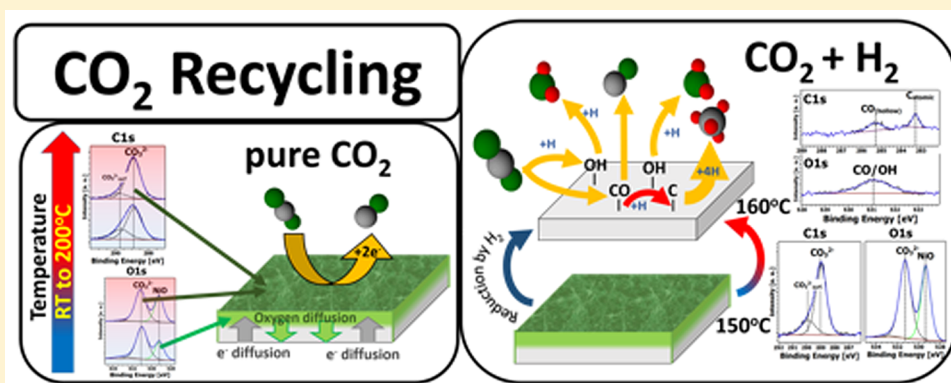
# Recycling of CO<sub>2</sub>: Probing the Chemical State of the Ni(111) Surface during the Methanation Reaction with Ambient-Pressure X-Ray Photoelectron Spectroscopy

Christian Heine,<sup>†</sup> Barbara A. J. Lechner,<sup>†,†</sup> Hendrik Bluhm,<sup>‡</sup> and Miquel Salmeron<sup>\*,†,§</sup>

<sup>†</sup>Materials Sciences and <sup>‡</sup>Chemical Sciences Division, Lawrence Berkeley National Laboratory, 1 Cyclotron Road, Berkeley, California 94720, United States

<sup>§</sup>Department of Materials Science and Engineering, University of California, Berkeley, California 94720, United States

 Supporting Information



**ABSTRACT:** Using ambient-pressure X-ray photoelectron spectroscopy (AP-XPS), we studied the adsorption and reactions of CO<sub>2</sub> and CO<sub>2</sub> + H<sub>2</sub> on the Ni(111) surface to identify the surface chemical state and the nature of the adsorbed species during the methanation reaction. In 200 mTorr CO<sub>2</sub>, we found that NiO is formed from CO<sub>2</sub> dissociation into CO and atomic oxygen. Additionally, carbonate (CO<sub>3</sub><sup>2-</sup>) is present on the surface from further reaction of CO<sub>2</sub> with NiO. The addition of H<sub>2</sub> into the reaction environment leads to reduction of NiO and the disappearance of CO<sub>3</sub><sup>2-</sup>. At temperatures >160 °C, CO adsorbed on hollow sites, and atomic carbon and OH species are present on the surface. We conclude that the methanation reaction proceeds via dissociation of CO<sub>2</sub>, followed by reduction of CO to atomic carbon and its hydrogenation to methane.

## 1. INTRODUCTION

Fossil fuels such as oil, natural gas, and coal are major energy sources and starting materials for a great variety of products in the chemical industry. However, the use of fossil fuels brings with it several problems since they are a limited resource and their combustion results in CO<sub>2</sub> emission, which is largely responsible for the greenhouse effect.

One strategy to alleviate these problems is the chemical recycling of CO<sub>2</sub>, a topic that has been discussed in several recent review articles.<sup>1–5</sup> This approach involves the hydrogenation of CO<sub>2</sub> by renewably generated hydrogen to produce methanol, CO (used in syngas), methane, and other precursors. An important example is the Sabatier reaction (methanation reaction): CO<sub>2</sub> + 4H<sub>2</sub> → CH<sub>4</sub> + 2 H<sub>2</sub>O,<sup>6</sup> for which nickel is one of the most commonly used catalysts.<sup>2,4,7,8</sup> Despite numerous experimental and theoretical studies, the mechanism of the CO<sub>2</sub> methanation reaction is not yet fully understood. Prior kinetic investigations suggested the formation of CO which is then converted to methane, CH<sub>4</sub>.<sup>9–12</sup> The mechanism of the reverse water–gas shift reaction (RWGS), forming CO from CO<sub>2</sub> (CO<sub>2</sub> + H<sub>2</sub> → CO + H<sub>2</sub>O), was suggested to

proceed via formation of a surface carbonate, CO<sub>3</sub><sup>2-</sup>, followed by a formate intermediate, HCO<sub>2</sub><sup>-</sup>.<sup>13</sup> Alternatively, direct dissociation of CO<sub>2</sub> into CO and atomic oxygen was suggested,<sup>10</sup> followed by reduction of CO to atomic carbon, which is then hydrogenated by atomic hydrogen adsorbed on the Ni surface.<sup>14,15</sup> The energetics of the dissociative pathway and subsequent hydrogenation of atomic carbon was examined with density functional theory (DFT) on Ni(111).<sup>14–16</sup> Thus, experimental investigations of the adsorption and hydrogenation behavior of CO<sub>2</sub> on Ni(111) can be compared with the DFT calculations to obtain an in-depth insight into the methanation reaction mechanism.

Because of its weak binding, CO<sub>2</sub> was only found to physisorb on Ni(111) under ultra-high-vacuum (UHV) conditions at low temperatures (below –173 °C).<sup>17,18</sup> When the Ni(111) surface is pre-covered with oxygen, however, carbonate formation can already be observed at room temperature (RT).<sup>17–20</sup> DFT calculations predict that the

Received: July 5, 2016

Published: September 6, 2016

chemisorption of CO<sub>2</sub> on Ni(111) is not energetically favored,<sup>21</sup> but the dissociation products, CO and atomic oxygen, bind strongly to nickel. In contrast, on the Ni(110) surface CO<sub>2</sub> chemisorption is strong,<sup>21</sup> and its dissociation to CO and atomic oxygen is observed even under UHV conditions.<sup>18,22–27</sup> The CO<sub>2</sub> chemistry is thus remarkably different on Ni(111) and Ni(110). The activation of the weakly bound CO<sub>2</sub> on Ni(111) by thermal dissociation, therefore, requires a suitable pressure of CO<sub>2</sub> gas to maintain a sufficient CO<sub>2</sub> coverage (in equilibrium with the gas) for dissociation to occur at an appreciable rate. An ambient-pressure X-ray photoelectron spectroscopy (AP-XPS)<sup>28–33</sup> investigation is therefore a very appropriate technique to study the Ni(111) surface composition under such reaction conditions and to address the role of gas pressure in the adsorption/dissociation and methanation properties of CO<sub>2</sub> on that surface.

In this Article, we present an AP-XPS study of the CO<sub>2</sub> interaction with the Ni(111) surface in the temperature range between RT and 200 °C at 200 mTorr. The C1s, O1s, and Ni2p<sub>3/2</sub> core-level spectra revealed the presence of NiO and NiCO<sub>3</sub>, indicating that CO<sub>2</sub> does indeed dissociate under these conditions. Furthermore, we investigated the reaction of CO<sub>2</sub> with H<sub>2</sub> in a 1:1 ratio at temperatures up to 300 °C. The reaction produced CO and atomic carbon, which were detected on the surface at 160 °C, thus confirming the dissociative reaction pathway.

## 2. EXPERIMENTAL SECTION

To eliminate complications arising from segregation of dissolved carbon in the bulk, we first depleted the Ni(111) crystal from carbon by repeated cycles (≥30) of Ar<sup>+</sup> sputtering (15–30 min, 1 keV) and annealing at 600 °C (10 min). A clean Ni(111) surface was produced, as verified by examination of the XPS C 1s peak region, which showed no peak above the noise level under UHV conditions. This surface produced a sharp hexagonal low-energy electron diffraction (LEED) pattern.

The AP-XPS experiments were performed at beamline 11.0.2<sup>34</sup> of the Advanced Light Source in Berkeley. An important requirement for experiments with reactive metals such as Ni is to achieve a clean chamber environment to prevent adventitious contamination, in particular of molecules containing C and O. We achieved this by igniting a nitrogen plasma prior to conventional bake-out, which is effective in stripping adsorbates from the chamber walls that can be later displaced when reactant gases are introduced. The base pressure in both the preparation and high-pressure (HP) XPS chambers was in the lower 10<sup>–10</sup> Torr range. Subsequently, H<sub>2</sub> and CO<sub>2</sub> were introduced into the chamber through leak valves, with minimal desorption of gases from the walls of the chamber. The pressure was measured with MKS722A Baratron capacitance and Granville Phillips 275 Convectron Pirani pressure gauges. It is well known that hot filaments, like those of ion pressure gauges, form CO.<sup>35</sup> Indeed, we observed detectable CO contamination on the Ni(111) surface, even under UHV conditions, with a hot filament in the background. Furthermore, CO<sub>2</sub> can split into CO and atomic oxygen on hot filaments, which can lead to misleading XPS results. We will comment on this effect in the Results section. Consequently, the ion gauges were switched off during and after the cleaning steps. Additional precautions included (a) defocusing the X-ray beam to avoid beam-induced reactions, (b) blocking the X-ray beam by a shutter after every core-level measurement, and (c) moving the X-ray spot position to a new fresh position on the sample between core-level measurements. Survey spectra were acquired at a photon energy ( $E_{ph}$ ) of 735 eV to check for contamination before the collection of high-resolution spectra. A survey spectrum under UHV conditions and the corresponding LEED pattern are shown in the Supporting Information, Figure S1.

Photon energies of 1080 eV for Ni2p, 735 eV for O1s, and 490 eV for C1s were used to produce photoelectrons with kinetic energies

( $E_{kin}$ ) around 200 eV for core-level spectra, corresponding to inelastic mean free paths (IMFPs) of approximately 0.5 nm, for metallic Ni.<sup>36</sup> We also investigated each core level with higher photon energies, i.e., 1410 eV for Ni2p, 1080 eV for O1s, and 835 eV for C1s, to create photoelectrons with  $E_{kin} = 550$  eV, corresponding to an IMFP of ~1 nm, to obtain a depth profile under selected conditions. The peak position energies are always referred to the Fermi level ( $E_f$ ) measured in the same spectrum. Details of the fitting procedure will be given in the Results part.

The values shown in Table 1 are computed in the following way. In case of the Ni2p<sub>3/2</sub>, the areas of all component peaks (main line +

**Table 1. Atomic Percentages of Metallic Ni, NiO, and NiCO<sub>3</sub> Calculated from the Ni2p<sub>3/2</sub> Core Level Peak Areas and the Ratios of the NiO Peak to the NiCO<sub>3</sub> Peak As Deduced from the Ni2p<sub>3/2</sub> and O1s Spectra**

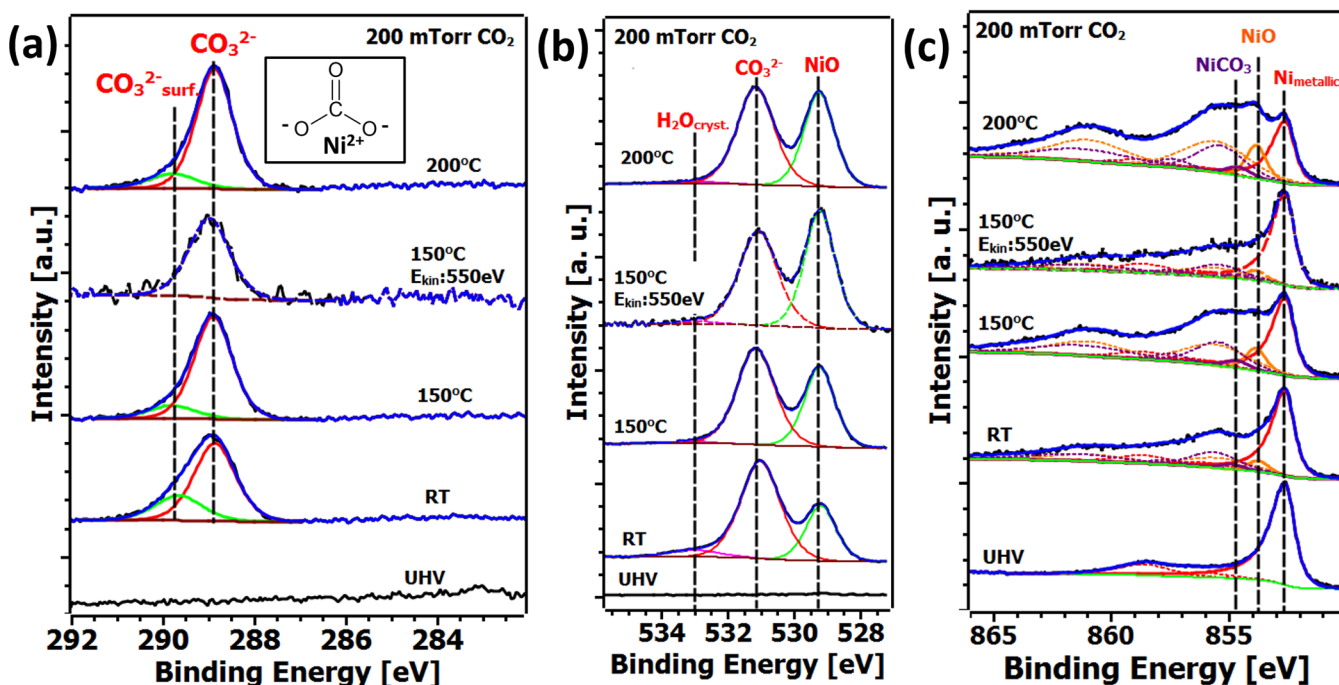
conditions	% Ni <sup>0</sup>	% NiO	% NiCO <sub>3</sub>	NiO/NiCO <sub>3</sub> ratio	
				from Ni2p <sub>3/2</sub>	from O1s
200 mTorr CO <sub>2</sub> at RT	49	24	27	0.89	0.43
200 mTorr CO <sub>2</sub> at 150 °C	33	37	30	1.2	0.66
200 mTorr CO <sub>2</sub> at 200 °C	22	47	31	1.53	0.8
200 mTorr CO <sub>2</sub> at 150 °C ( $E_{kin} = 550$ eV)	55	22	23	1.0	1.0

satellite line) corresponding to a specific species, e.g., NiO, were added. The main line and the corresponding satellite lines belong to the same chemical ground state. In the case of charge-transfer satellites, additional photo emission lines may appear due to different screening situations. Excitation of plasmons during the photoelectron excitation can generate distinct satellite lines. Both types of satellites have been discussed in the literature for chemical species of Ni.<sup>37,38</sup> The peak areas of each chemical species are then normalized to the peak area of the Ni2p<sub>3/2</sub>, and the ratio is given in terms of atomic percentage.<sup>39</sup> Since the ionization cross-section, inelastic mean free path, and transmission function of the analyzer are the same for the each chemical species, the ratio eliminates these parameters from the estimation. The same is true for the ratio of NiO/NiCO<sub>3</sub> deduced from the Ni2p<sub>3/2</sub> and O1s.

## 3. RESULTS AND DISCUSSION

**3.1. Ni(111) in 200 mTorr CO<sub>2</sub>.** Figure 1 shows the C1s (a), O1s (b), and Ni2p<sub>3/2</sub> (c) spectra in 200 mTorr of CO<sub>2</sub> (except the bottom spectrum, acquired under UHV conditions). The spectra correspond to the surface state at increasing temperatures: RT, 150 °C, and 200 °C. The XP spectra in the O1s and C1s regions show no peaks above the noise level (bottom curves in (a) and (b)), and the Ni2p could be fitted with the Doniac–Sunjic line shape of metallic nickel, confirming a clean initial surface. A detailed description of the analysis of each core level is presented below.

In 200 mTorr of CO<sub>2</sub>, the C1s spectrum (Figure 1a) shows two components, at 288.9 ± 0.1 and 289.7 ± 0.1 eV binding energy (BE), respectively. Both components were fitted with Gaussian–Lorentzian peaks after subtraction of a Shirley background. The 289.7 eV peak decreases with respect to the 288.9 eV component after the temperature is increased to 150 and 200 °C. In addition to the surface-sensitive measurements at 200 eV kinetic energy (corresponding to an IMFP of 0.5 nm), we also measured the C1s spectrum at 150 °C with 550 eV kinetic energy (IMFP = 1 nm) to obtain a more bulk-sensitive measurement. The best fit in that case was obtained



**Figure 1.** Oxidation of Ni(111) in a CO<sub>2</sub> atmosphere. (a) C1s, (b) O1s, and (c) Ni2p<sub>3/2</sub> in 200 mTorr CO<sub>2</sub> in the temperature range from RT to 200 °C. All spectra are recorded at a kinetic energy of 200 eV, except where labels indicate a more bulk-sensitive measurement at  $E_{kin} = 550$  eV. Inset: Molecular structure of NiCO<sub>3</sub>.

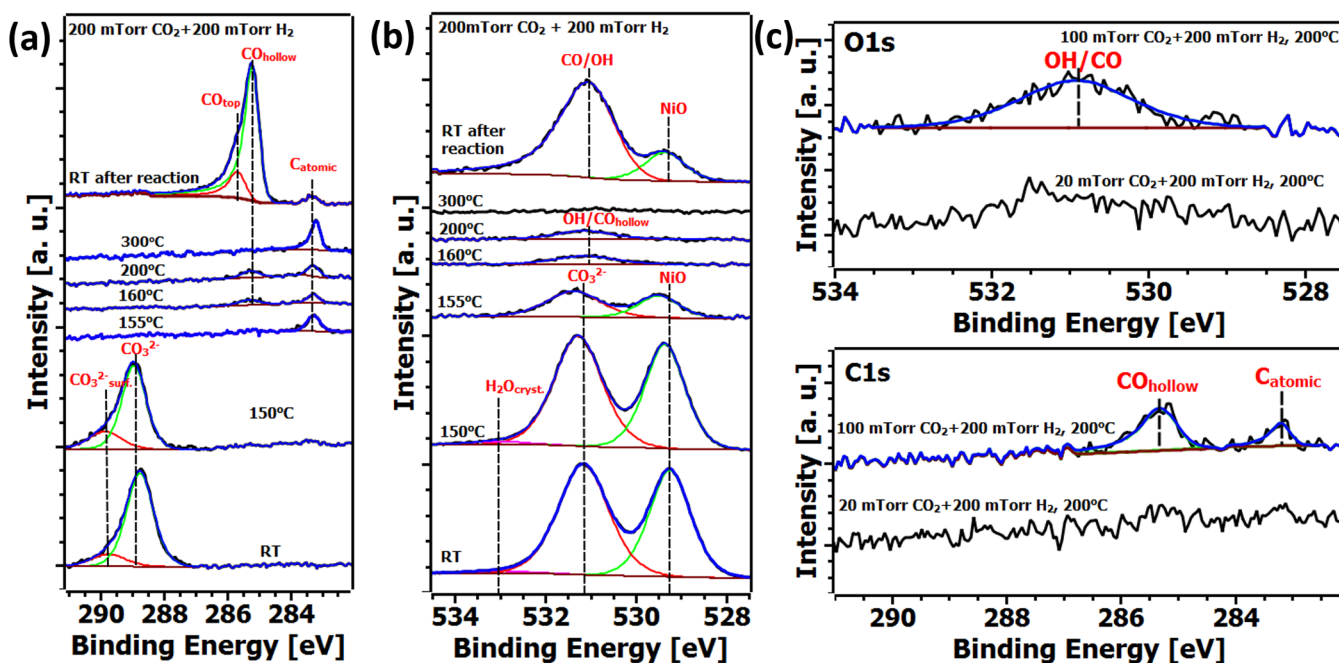
with a single component at  $289.0 \pm 0.1$  eV, which is within the error bar of the 288.9 eV component observed in the more surface-sensitive spectra. Thus, we assign the 289.7 eV peak to a surface species.

The 288.9 eV component of the C1s spectrum can be assigned to a carbonate species, in agreement with the carbonate peak at 289 eV BE reported previously.<sup>17,40,41</sup> Under UHV conditions, carbonate does not form on the clean Ni(111) surface;<sup>17,18</sup> it forms only after pre-adsorption of oxygen.<sup>17–19,40,41</sup> The species observed at 289.7 eV has not been reported in the literature so far. In our experiments, we observe the formation of carbonate by dosing CO<sub>2</sub> in the mTorr pressure range because under this pressure, at RT, CO<sub>2</sub> dissociates ( $\text{CO}_2 \rightarrow \text{CO}_{\text{ads}} + \text{O}_{\text{ads}}$ ), followed by reaction of the atomic oxygen with another CO<sub>2</sub> molecule. To test whether the 289.7 eV peak could result from CO adsorbed on the carbonate-covered surface, we formed the carbonate structure on Ni(111) at RT in a separate experiment. Subsequently, we evacuated the chamber and introduced CO at different pressures up to 100 mTorr. The resulting C1s spectrum, shown in the Supporting Information, Figure S2, shows no significant changes in the 289.7 eV peak intensity. Therefore, we can conclude that this species is not due to CO adsorption on the carbonate covered surface. This finding is in line with CO adsorption experiments on NiO reported in the literature<sup>42</sup> and indicates that CO does not stick to NiO nor NiCO<sub>3</sub> at RT.<sup>17,42</sup> Therefore, we interpret the 289.7 eV component as another carbonate species.

The O1s spectra in Figure 1b can be fitted by three Gaussian–Lorentzian peaks after subtraction of a Shirley background. The components are located at  $529.2 \pm 0.1$ ,  $531.1 \pm 0.1$ , and  $533.1 \pm 0.1$  eV BE, respectively. The 529.2 eV peak increases with increasing temperature from RT to 200 °C compared to the peak at 531.1 eV, while the 533.1 eV component is reduced at higher temperatures. The spectrum

recorded with 550 eV kinetic energy shows an inverted peak intensity ratio of the 531.1 and the 529.2 eV components in comparison to the spectrum recorded at 200 eV kinetic energy. We thus conclude that the 529.2 eV species, which we identify as NiO,<sup>17,43</sup> is located beneath the 531.1 eV species. It was previously reported that chemisorbed oxygen on Ni(111) has the same peak position as in NiO,<sup>17,44</sup> but instead of the symmetric peak profile characteristic of semiconductors and insulators, the line shape is asymmetric for the chemisorbed species due to the interaction of chemisorbed oxygen with the high d-density of states at the Fermi level in metallic Ni.<sup>44</sup> To confirm this finding, we formed a  $p(2 \times 2)$  oxygen structure on Ni(111) and could indeed observe the asymmetric line shape in this control experiment, shown in Figure S3 along with the corresponding LEED pattern. Thus, the symmetric profile of the 529.2 eV peak seen in Figure 1b can be assigned to NiO. The formation of Ni oxide strongly suggests the dissociation of CO<sub>2</sub> as the origin of atomic oxygen. The 531.1 eV peak can be caused by either OH or carbonate on NiO,<sup>17,40,41</sup> which have similar BEs. The minority 533.1 eV species fits well with the peak position of adsorbed water on NiO,<sup>17,45</sup> which originates from residual water in the chamber. NiCO<sub>3</sub> appears always along with Ni(OH)<sub>2</sub> and crystallization water.<sup>46</sup> For comparison, nickel carbonate is approximately  $3\text{NiCO}_3 \cdot 2\text{Ni(OH)}_2 \cdot 4\text{H}_2\text{O}$ , and hydrated nickel carbonate is  $\text{NiCO}_3 \cdot 6\text{H}_2\text{O}$ . We thus assign the 533.1 eV peak to water associated with NiCO<sub>3</sub>–Ni(OH)<sub>2</sub> mixtures.

The Ni2p<sub>3/2</sub> core level contains several photoemission components, corresponding to different Ni chemical states,<sup>37,38</sup> as shown by the analysis of the O and C peaks discussed above. To fit the spectra in Figure 1c, we used a Shirley background with an offset for each spectrum. Initial values of the binding energies of Ni species were taken from the work of Grosvenor et al.<sup>38</sup> and Biesinger et al.<sup>37</sup> for (a) metallic Ni at 852.6 eV and two satellite lines, (b) NiO at 853.7 eV and four satellite lines,



**Figure 2.** In situ XPS measurements of the chemical state of a model Ni(111) catalyst surface during CO<sub>2</sub> reduction. (a) C1s and (b) O1s spectra in 200 mTorr CO<sub>2</sub> and 200 mTorr H<sub>2</sub> in the temperature range from RT to 300 °C. (c) O1s and C1s spectra in 20 mTorr CO<sub>2</sub> + 200 mTorr H<sub>2</sub> and in 100 mTorr CO<sub>2</sub> + 200 mTorr H<sub>2</sub> (the CO<sub>2</sub> pressure was increased from 10 to 100 mTorr) at 200°C.

and (c) NiCO<sub>3</sub> (similar to that in NiOH) at 854.9 eV and five satellite lines. We then let the peak energies and the full width at half-maximum of the main lines vary to achieve the best fit. The relative peak ratio and energies of the satellites to the main lines were kept constant. We found that, in all spectra, the peak position of the main lines after optimization was within  $\pm 0.1$  eV of the literature values given above. The Ni2p<sub>3/2</sub> spectrum under UHV conditions was fitted with components related to metallic nickel only. As can be seen in Figure 1c, the intensities of the NiO and NiCO<sub>3</sub> components increase with temperature relative to that of the metallic component. The spectrum taken with 550 eV kinetic energy (bulk-sensitive) at 150 °C shows decreased intensities of the NiO and NiCO<sub>3</sub> peaks in comparison to the surface-sensitive measurements at 200 eV kinetic energy. The normalized intensities of the various Ni components and the ratio of the NiO and NiCO<sub>3</sub> deduced from the Ni2p<sub>3/2</sub> and O1s peak areas are given in Table 1 for the final discussion of the core-level analysis in 200 mTorr CO<sub>2</sub>.

From Table 1, we see that the fraction of metallic nickel is reduced, while that of NiO increases and that of NiCO<sub>3</sub> remains approximately constant, with increasing temperature in 200 mTorr CO<sub>2</sub>. From the comparison of the ratio of the NiO peak to the NiCO<sub>3</sub> peak deduced from the Ni2p<sub>3/2</sub> and O1s, we find that this result is in line with the O1s analysis. The values of both ratios are different by about a factor 2, as expected from the different stoichiometry of oxygen in NiO and NiCO<sub>3</sub>, as shown in the Figure 1a, inset showing Ni<sup>2+</sup> coordinated to two oxygen atoms in NiCO<sub>3</sub> and to one oxygen atom in NiO. The ratio of NiO/NiCO<sub>3</sub> deduced from the Ni2p<sub>3/2</sub> peak at 550 eV kinetic energy has a large uncertainty due to the low signal-to-noise ratio and the strong metallic component. We therefore rely here on the ratio from the O1s spectrum.

We interpret the XPS of Ni(111) in 200 mTorr CO<sub>2</sub> in the temperature range from RT to 200 °C as follows. The appearance of NiO clearly indicates the dissociation of CO<sub>2</sub>

into CO and chemisorbed oxygen (precursor for the formation of NiO). This result fits well with prior DFT calculations, which showed that chemisorption of molecular CO<sub>2</sub> is not energetically favored while its dissociation is exothermic.<sup>21</sup> The activation barrier between intact physisorbed CO<sub>2</sub> and the dissociation products CO and O explains the need for a sufficiently high pressure of CO<sub>2</sub>. Only under such conditions a sufficient population of CO<sub>2</sub> in the initial molecular state can be obtained at RT for a measurable rate of thermally activated dissociation. At cryogenic temperatures in UHV, only the molecular physisorbed state is obtained, which desorbs upon heating well before RT. The same phenomenon was observed for CO<sub>2</sub> on Ru(0001), where molecular CO<sub>2</sub> desorbs around 250 K.<sup>47</sup> The increased dissociative adsorption of CO<sub>2</sub> at RT leads to oxide formation, where Ni<sup>0</sup> is oxidized to Ni<sup>2+</sup> and CO<sub>2</sub> is reduced to CO. Since CO cannot adsorb on either NiO or NiCO<sub>3</sub> at RT<sup>17,42</sup> (see Supporting Information), the CO formed in the dissociation process immediately desorbs.

Carbonate is formed by further reaction of NiO with CO<sub>2</sub>. The two peaks in the C 1s spectra are assigned to NiCO<sub>3</sub> (289.7 and 288.9 eV). The 289.7 eV component decreases in intensity with increasing temperature. Gordon et al.<sup>19</sup> found two CO<sub>2</sub> peaks in temperature-programmed desorption (TPD) experiments, at 120 and 370 °C, after forming carbonate on pre-oxidized Ni(111) at RT. Carbonate formed at temperatures above 150 °C shows just one desorption peak. This TPD result is in line with our observation of one carbonate species at 288.9 eV and a second less stable one at 289.7 eV.

The surface fraction of NiO increases with increasing temperature in the presence of CO<sub>2</sub>, as evident in the growing NiO peaks in the O1s and Ni2p<sub>3/2</sub> spectral regions at higher temperatures. Furthermore, the bulk-sensitive O1s measurement shows also an increased NiO intensity, indicative of bulk oxidation. Since electrons are needed for the CO<sub>2</sub> dissociation process, oxygen has to diffuse into the bulk and consume metallic nickel to form NiO, which cannot provide electrons in

its oxidation state (2+) and is known to be a p-type semiconductor.<sup>48,49</sup>

A chemisorbed state of CO<sub>2</sub> could not be found in the present study, in agreement with DFT calculations which predict that CO<sub>2</sub> chemisorption is not energetically favored on Ni(111).<sup>21</sup> Furthermore, chemisorbed oxygen from the CO<sub>2</sub> dissociation, which was observed on Ni(110) under ambient pressure conditions,<sup>27</sup> was not observed here. Instead, on Ni(111), oxide is formed.

Our results differ significantly from those of Roiaz et al.<sup>27</sup> and Monachino et al.<sup>20</sup> where, under similar conditions of CO<sub>2</sub> in the mTorr range, multiple carbon species were observed on a Ni(110) crystal at 150 °C, with BE ranging from 283 to 290 eV, assigned to different carbon species including atomic carbon, graphene, and carbonate. The difference could be a result from the significantly different reactivity of the Ni(110) surface, as reported in the Introduction. However, in a test experiment, we could obtain spectra similar to those reported by Roiaz et al.<sup>27</sup> under similar conditions (same temperature and pressure range) when the Ni(111) surface was exposed to CO and other gases produced from hot filaments in the chamber (Figure S4).

**3.2. Ni(111) in a Reaction Environment: 200 mTorr CO<sub>2</sub> + 200 mTorr H<sub>2</sub>.** After cooling the sample from 200 °C to RT in the presence of 200 mTorr CO<sub>2</sub>, we introduced 200 mTorr of H<sub>2</sub> in the chamber. To investigate the RWGS and methanation reactions and to identify possible reaction intermediates, we monitored the photoelectron spectra while gradually increasing the temperature from RT to 300 °C. The resulting C1s and O1s XPS regions are shown in Figure 2. From RT to 150 °C, only the carbonate peaks produced by CO<sub>2</sub> dissociation were apparent in the C1s spectrum. When the temperature was increased from 150 to 155 °C, however, the carbonate peaks disappeared while a new peak appeared at 283.3 ± 0.1 eV, followed by another component at 285.2 ± 0.1 eV at 160 °C. After the temperature was further increased to 200 °C, both peaks were still present. After further heating to 300 °C, only the peak at 283.3 eV remained with increased intensity. After cooling back to RT in the reaction gas environment, the component at 285.2 eV together with a shoulder at 285.8 eV reappeared with strongly increased intensity. The peak at 283.3 eV is also evident in the spectrum but with reduced peak intensity. The 283.3 eV component fits well with the literature value for atomic carbon.<sup>50</sup> The two new peaks at 285.2 and 285.8 eV were fitted with an asymmetric peak profile after subtraction of a Shirley background. The new component at 285.2 eV in the C1s region can be assigned to CO adsorbed on hollow sites of the Ni(111) surface,<sup>51</sup> while the shoulder at 285.8 ± 0.1 eV is close to the literature value (285.9 eV) for CO adsorbed on top sites.<sup>51</sup> The C1s and O1s spectra of CO adsorbed on Ni(111) have asymmetric peak shapes due both to the interaction of CO with the high density of state of metallic Ni and to shakeup lines originating from different vibrational states.<sup>52</sup> We confirmed these assignments with a reference experiment shown in the Supporting Information, Figure S5, where the same peak positions were obtained when a clean Ni(111) surface was exposed to 20 mTorr CO. After evacuation of the HP chamber, only the peak at 285.2 eV, corresponding to CO on hollow sites, was observed, in agreement with the literature.<sup>21</sup> The top site CO peak (285.8 eV) disappeared after evacuation of the chamber, indicative of weaker bonding to the Ni(111) surface.

The two C1s spectra before and after temperature treatment clearly look different. In the initial state carbonate is the

predominant species, while in the final state (after reaction) the surface is covered with CO. This is, however, a temporary poisoning of the surface by the CO product, a result of the kinetics of NiO formation. As the NiO surface fraction grows with time (on the scale of minutes at RT), CO is displaced from the surface, and the spectrum returns to the initial one shown at the bottom of the figure.

To verify this, we performed an additional experiment where the sample was cooled from 200 to 150 °C in CO<sub>2</sub> and H<sub>2</sub> (see Supporting Information, Figure S6). At 200 °C, the spectrum revealed CO on hollow sites and atomic carbon. At 150 °C, CO was still present on top as well as hollow sites. However, the NiO component in the O1s spectra increased with time, while the CO components in the C1s region disappeared and the peak at 288.9 eV grew, indicating carbonate species formation, similar to the results shown in Figure 1a. At 150 °C, H<sub>2</sub> was not able to reduce the surface, in agreement with the spectrum in Figure 2a,b.

The corresponding O1s spectra are shown in Figure 2b. At RT and 150 °C, the spectra exhibit the same components observed in a pure CO<sub>2</sub> atmosphere, corresponding to crystallization water, NiCO<sub>3</sub>, and NiO. When the temperature was increased to 155 °C, the NiCO<sub>3</sub> and NiO components strongly decreased in intensity, and the water component disappeared entirely. As can be seen, the transition from oxidized to metallic Ni at 155 °C is sharp. This is due to the fact that we are reducing only a very thin oxide where, as shown in Figure 1c, the metallic component in the Ni2p<sub>3/2</sub> core level at  $E_{\text{kin}} = 550$  eV, which samples one or two surface layers, is very strong. It also indicates a low activation barrier that makes the reaction fast.

At 160–200 °C, only a weak peak is present at 531.1 ± 0.1 eV BE, similar to that of oxygen in NiCO<sub>3</sub>. At 300 °C, no peak can be seen in the O1s region. After the sample was cooled back down to RT, the NiO component reappeared and grew with time, together with a broad component at 531 eV BE, which we fitted with just one asymmetric component after a Shirley background subtraction. We assign the small peak at 531.1 eV in the O1s spectrum at 160 and 200 °C to CO and OH groups, which have similar peak positions in the O1s spectrum.<sup>17,51</sup> Although the oxygen in the carbonate has a similar BE, it can be excluded because no carbonate peak was found in the C1s spectrum at these temperatures. The O1s spectrum, after the sample cooled down, was fitted with a symmetric component for NiO at 529.2 eV and another, asymmetric component at 531.1 eV, assigned to CO (which can be found in the C1s spectrum) and/or OH groups on metallic nickel, respectively. The Ni2p<sub>3/2</sub> core level (not shown) exhibits a metallic nickel signature when the carbonate structure disappears (155–300 °C).

The C1s and O1s spectra in Figure 2a,b can be interpreted as follows. At 155 °C, the NiCO<sub>3</sub> and NiO species are reduced by hydrogen, indicating that H<sub>2</sub> dissociates at this temperature to reduce the carbonate and oxide species. We note that CO does not appear yet on the surface at this temperature, presumably because sufficient oxide remains on the surface. The atomic carbon formed under these conditions most likely results from carbonate decomposition. At 160 °C, CO appears on the Ni(111) surface, indicating that the RWGS reaction (CO<sub>2</sub> + H<sub>2</sub> → CO + H<sub>2</sub>O) is occurring. Further evidence for the RWGS reaction is provided by the OH peak (531.1 eV) in the O1s spectrum (Figure 2b), as OH is an intermediate in the production of water. CO can also be a possible source of atomic

carbon on Ni(111), as it adsorbs strongly on hollow sites<sup>21</sup> and can therefore be further reduced to atomic carbon. A further increase of the temperature to 300 °C promotes the reduction of some of the CO to atomic carbon, evident in the increased peak intensity at 283.3 eV. The fact that CO is a source for atomic carbon is supported by the spectra in Figure 2c, which we discuss below. After the sample was cooled to RT, a large CO peak with the main component assigned to CO on hollow sites and a second component assigned to CO on top sites is seen in the C1s spectrum. We interpret this as resulting either from re-adsorption of gas-phase CO produced by the RWGS reaction or from CO that remains adsorbed during cooling. As explained above, our reference experiment (Supporting Information) indicates that CO is removed by the growing NiO.

We also conducted experiments with different CO<sub>2</sub>:H<sub>2</sub> ratios in the gas phase. In Figure 2c, the C1s and O1s spectra in 20 mTorr CO<sub>2</sub> + 200 mTorr H<sub>2</sub> and in 100 mTorr CO<sub>2</sub> + 200 mTorr H<sub>2</sub> are shown. With 20 mTorr CO<sub>2</sub> in the reaction gas, the CO concentration is too low to be detected by XPS in the C1s region. Similarly, the O1s region does not exhibit any peak that would indicate the occurrence of the RWGS reaction. When the CO<sub>2</sub> concentration was increased to 100 mTorr, a peak from CO on hollow sites was observed, accompanied by atomic carbon in the C1s spectrum. In addition, a broad OH/CO peak can be seen in the O1s spectrum under these conditions. These results confirm that atomic carbon appears in the presence of CO, indicative of the further reduction of CO. Atomic carbon is the most plausible source of methane formed in the Sabatier reaction ( $\text{CO}_2 + 4\text{H}_2 \rightarrow \text{CH}_4 + 2\text{H}_2\text{O}$ ),<sup>14–16</sup> suggesting that the reaction occurs by first CO<sub>2</sub> reduction to CO, which is then further reduced to atomic carbon, before finally being hydrogenated to methane. These findings are different from the work of Roiaz et al.<sup>27</sup> and Monachino et al.<sup>20</sup> on Ni(110). Almost no CO was found on the Ni(110) surface in a 9:1 feed of H<sub>2</sub> and CO<sub>2</sub>. Instead, a much larger amount of atomic carbon and extended sp<sup>2</sup> carbon modifications are found. The Ni(110) seems to convert CO much easier to atomic carbon than Ni(111).

#### 4. CONCLUSION

Our AP-XPS study provides a detailed insight into the reactions occurring on a Ni(111) surface in the presence of CO<sub>2</sub> and in CO<sub>2</sub> + H<sub>2</sub> environments in the mTorr range. In pure CO<sub>2</sub> gas, NiO formation can be observed even at RT, demonstrating that CO<sub>2</sub> dissociates into CO and atomic oxygen. The process requires transfer of two electrons from metallic Ni to the CO<sub>2</sub> molecule, the Ni becoming oxidized to Ni<sup>2+</sup> while CO<sub>2</sub> is reduced to CO, a redox reaction involving electrons from metallic Ni. The CO binds too weakly on NiO/NiCO<sub>3</sub> and is thus released to the gas phase. A temperature increase accelerates the CO<sub>2</sub> dissociation process, evident in the increased oxide peak intensity in the O1s spectra and the increase of NiO concentration revealed by the Ni2p<sub>3/2</sub> spectra. Carbonate is formed as a result of the further reaction of NiO with CO<sub>2</sub>. The AP-XPS investigation shows that the CO<sub>2</sub> molecule can be activated on Ni(111) at sufficient high pressures, which cannot be achieved under UHV conditions.<sup>17,18</sup>

After addition of H<sub>2</sub> to the gas environment, the NiO and NiCO<sub>3</sub> species are reduced at an increased rate at 155 and 160 °C, while oxide and carbonate species disappear from the surface, leaving chemisorbed CO temporarily on the surface. A

weak peak centered at 531.1 eV in the O1s spectrum from OH and CO indicates that the RWGS reaction occurs under these conditions. Furthermore, the presence of atomic carbon (peak at 283.3 eV) indicates that the methanation reaction mechanism on the Ni(111) surface involves the reduction of CO to atomic carbon, which is then hydrogenated to methane.<sup>14–16</sup> Finally, it should be noted that the practical methanation catalyst is Ni supported usually on silica.<sup>4</sup> It is generally discussed that the support can have an influence on the reaction mechanism.<sup>4,8</sup> A possible model system to investigate the effect of the support with XPS could be Ni particles deposited on very thin silica to prevent charging.<sup>53</sup>

#### ■ ASSOCIATED CONTENT

##### Supporting Information

The Supporting Information is available free of charge on the ACS Publications website at DOI: 10.1021/jacs.6b06939.

Survey spectrum of a clean Ni(111) surface under UHV conditions with LEED pattern; C1s spectra of CO dosing onto carbonate formed on Ni(111) at room temperature; O1s spectrum of oxygen p(2×2) reconstruction on Ni(111); C1s spectra of CO-induced contamination on Ni(111) and its effects on the CO<sub>2</sub>/Ni(111) interaction; C1s and O1s spectra of CO adsorption on Ni(111) in the mTorr range; and O1s and C1s spectra after cooling from 200 to 150 °C in 200 mTorr CO<sub>2</sub> and 200 mTorr H<sub>2</sub> (PDF)

#### ■ AUTHOR INFORMATION

##### Corresponding Author

\*mbsalmeron@lbl.gov

##### Present Address

<sup>†</sup>B.A.J.L.: Chemistry Department, Technische Universität München, Lichtenbergstraße 4, Garching 85748, Germany

##### Notes

The authors declare no competing financial interest.

#### ■ ACKNOWLEDGMENTS

This work was supported by the Integrated Mesoscale Architectures for Sustainable Catalysis (IMASC), an Energy Frontier Research Center funded by the U.S. Department of Energy (DOE), Office of Science, Basic Energy Sciences, under Award No. DE-SC0012573. It used resources of the Advance Light Source, a user Facility supported by the Office of Science of the U.S. DOE under Contract DE-AC02-05CH11231.

#### ■ REFERENCES

- (1) Olah, G. A.; Goepfert, A.; Prakash, G. K. S. *Angew. Chem., Int. Ed.* **2005**, *44*, 2636.
- (2) Centi, G.; Perathoner, S. *Catal. Today* **2009**, *148* (3–4), 191.
- (3) Schlögl, R. *Angew. Chem.* **2015**, *127* (15), 4512.
- (4) Wang, W.; Wang, S.; Ma, X.; Gong, J. *Chem. Soc. Rev.* **2011**, *40* (7), 3703.
- (5) Hoekman, S. K.; Broch, A.; Robbins, C.; Purcell, R. *Int. J. Greenhouse Gas Control* **2010**, *4* (1), 44.
- (6) Sabatier, P. *Ind. Eng. Chem.* **1926**, *18* (10), 1005.
- (7) Du, G.; Lim, S.; Yang, Y.; Wang, C.; Pfefferle, L.; Haller, G. L. *J. Catal.* **2007**, *249* (2), 370.
- (8) Schlögl, R. *Angew. Chem., Int. Ed.* **2015**, *54* (11), 3465.
- (9) Falconer, J. L.; Ercüment Zağlı, A. *J. Catal.* **1980**, *62* (2), 280.
- (10) Weatherbee, G. D.; Bartholomew, C. H. *J. Catal.* **1982**, *77* (2), 460.

- (11) Peebles, D. E.; Goodman, D. W.; White, J. M. *J. Phys. Chem.* **1983**, *87* (22), 4378.
- (12) Lapidus, A. L.; Gaidai, N. A.; Nekrasov, N. V.; Tishkova, L. A.; Agafonov, Y. A.; Myshenkova, T. N. *Pet. Chem.* **2007**, *47* (2), 75.
- (13) Marwood, M.; Doepper, R.; Renken, A. *Appl. Catal., A* **1997**, *151* (1), 223.
- (14) Watwe, R. M.; Bengaard, H. S.; Rostrup-Nielsen, J. R.; Dumesic, J. a; Norskov, J. K. *J. Catal.* **2000**, *189* (1), 16.
- (15) Ren, J.; Guo, H.; Yang, J.; Qin, Z.; Lin, J.; Li, Z. *Appl. Surf. Sci.* **2015**, *351*, 504.
- (16) Choe, S.; Kang, H.; Kim, S. *Bull. Korean Chem. Soc.* **2005**, *26* (11), 1682.
- (17) Lorenz, M. Interaction of small molecules with thin NiO layers and related metal surfaces studied with high resolution X-ray photoelectron spectroscopy. Ph.D. Thesis, Friedrich-Alexander-Universität: Erlangen-Nürnberg, 2012.
- (18) Freund, H.-J.; Roberts, M. W. *Surf. Sci. Rep.* **1996**, *25* (8), 225.
- (19) Gordon, E. A.; Lambert, M. *Surf. Sci.* **1993**, *288*, 114.
- (20) Monachino, E.; Greiner, M.; Knop-Gericke, A.; Schlögl, R.; Dri, C.; Vesselli, E.; Comelli, G. *J. Phys. Chem. Lett.* **2014**, *5* (11), 1929.
- (21) Wang, S. G.; Cao, D. B.; Li, Y. W.; Wang, J.; Jiao, H. *J. Phys. Chem. B* **2005**, *109* (40), 18956.
- (22) Lindner, H.; Rupprecht, D.; Hammer, L.; Müller, K. *J. Electron Spectrosc. Relat. Phenom.* **1987**, *44* (1), 141.
- (23) Wambach, J.; Illing, G.; Freund, H. J. *Chem. Phys. Lett.* **1991**, *184* (1–3), 239.
- (24) Vesselli, E.; De Rogatis, L.; Ding, X.; Baraldi, A.; Savio, L.; Vattuone, L.; Rocca, M.; Fornasiero, P.; Peressi, M.; Baldereschi, A.; Rosei, R.; Comelli, G. *J. Am. Chem. Soc.* **2008**, *130* (34), 11417.
- (25) Dri, C.; Peronio, A.; Vesselli, E.; Africh, C.; Rizzi, M.; Baldereschi, A.; Peressi, M.; Comelli, G. *Phys. Rev. B: Condens. Matter Mater. Phys.* **2010**, *82* (16), 165403.
- (26) Vesselli, E.; Rizzi, M.; de Rogatis, L.; Ding, X.; Baraldi, A.; Comelli, G.; Savio, L.; Vattuone, L.; Rocca, M.; Fornasiero, P.; Baldereschi, A.; Peressi, M. *J. Phys. Chem. Lett.* **2010**, *1* (1), 402.
- (27) Roiaz, M.; Monachino, E.; Dri, C.; Greiner, M.; Knop-Gericke, A.; Schlögl, R.; Comelli, G.; Vesselli, E. *J. Am. Chem. Soc.* **2016**, *138* (110), 4146.
- (28) Bluhm, H.; Ogletree, D. F.; Fadley, C.; Hussain, Z.; Salmeron, M. *J. Phys.: Condens. Matter* **2002**, *14* (8), L227.
- (29) Salmeron, M.; Schlögl, R. *Surf. Sci. Rep.* **2008**, *63* (4), 169.
- (30) Schnadt, J.; Knudsen, J.; Andersen, J. N.; Siegbahn, H.; Pietzsch, A.; Hennies, F.; Johansson, N.; Mårtensson, N.; Öhrwall, G.; Bahr, S.; Mähl, S.; Schaff, O. *J. Synchrotron Radiat.* **2012**, *19* (5), 701.
- (31) Kaya, S.; Ogasawara, H.; Näslund, L. Å.; Forsell, J. O.; Casalongue, H. S.; Miller, D. J.; Nilsson, A. *Catal. Today* **2013**, *205*, 101.
- (32) Vass, E. M.; Hävecker, M.; Zafeirotos, S.; Teschner, D.; Knop-Gericke, A.; Schlögl, R. *J. Phys.: Condens. Matter* **2008**, *20* (18), 184016.
- (33) Starr, D. E.; Liu, Z.; Hävecker, M.; Knop-Gericke, A.; Bluhm, H. *Chem. Soc. Rev.* **2013**, *42* (13), 5833.
- (34) Frank Ogletree, D.; Bluhm, H.; Hebenstreit, E. D.; Salmeron, M. *Nucl. Instrum. Methods Phys. Res., Sect. A* **2009**, *601* (1–2), 151.
- (35) O'Hanlon, J. F. *A User's Guide to Vacuum Technology*, 3rd ed.; John Wiley & Sons, Inc.: Hoboken, NJ, 2003.
- (36) Tanuma, S.; Powell, C. J.; Penn, D. R. *Surf. Interface Anal.* **1994**, *21* (3), 165.
- (37) Biesinger, M. C.; Payne, B. P.; Lau, L. W. M.; Gerson, A.; Smart, R. S. C. *Surf. Interface Anal.* **2009**, *41* (4), 324.
- (38) Grosvenor, A. P.; Biesinger, M. C.; Smart, R. S. C.; McIntyre, N. S. *Surf. Sci.* **2006**, *600* (9), 1771.
- (39) Hesse, R.; Streubel, P.; Szargan, R. *Surf. Interface Anal.* **2005**, *37* (7), 589.
- (40) Behm, R. J.; Brundle, C. R. *Surf. Sci.* **1991**, *255* (3), 327.
- (41) Behm, R. J. *J. Vac. Sci. Technol., A* **1983**, *1* (2), 1223.
- (42) Wichtendahl, R.; Rodriguez-Rodrigo, M.; Härtel, U.; Kühlenbeck, H.; Freund, H. J. *Phys. Status Solidi Appl. Res.* **1999**, *173* (1), 93.
- (43) Uhlenbrock, S.; Scharfschwerdt, C.; Neumann, M.; Illing, G.; Freund, H.-J. *J. Phys.: Condens. Matter* **1992**, *4* (40), 7973.
- (44) Domnick, R.; Held, G.; Witte, P.; Steinrück, H. P. *J. Chem. Phys.* **2001**, *115* (4), 1902.
- (45) Carley, A. F.; Rassias, S.; Roberts, M. W. *Surf. Sci.* **1983**, *135*, 35.
- (46) Lascelles, K.; Morgan, L. G.; Nicholls, D.; Beyersmann, D. *Ullmann's Encyclopedia of Industrial Chemistry*; Wiley: Weinheim, 2012; Vol 24, p 117.
- (47) Feng, X.; Cerdá, J. I.; Salmeron, M. *J. Phys. Chem. Lett.* **2015**, *6* (9), 1780.
- (48) Fujimori, A.; Minami, F. *Phys. Rev. B: Condens. Matter Mater. Phys.* **1984**, *30* (2), 957.
- (49) Pizzini, S.; Morlotti, R. *J. Electrochem. Soc.* **1967**, *114* (11), 1179.
- (50) Patera, L. L.; Africh, C.; Weatherup, R. S.; Blume, R.; Bhardwaj, S.; Castellarin-Cudia, C.; Knop-Gericke, A.; Schloegl, R.; Comelli, G.; Hofmann, S.; Cepek, C. *ACS Nano* **2013**, *7* (9), 7901.
- (51) Held, G.; Schuler, J.; Sklarek, W.; Steinrück, H.-P. *Surf. Sci.* **1998**, *398* (1–2), 154.
- (52) Föhlisch, A.; Wassdahl, N.; Hasselström, J.; Karis, O.; Menzel, D.; Mårtensson, N.; Nilsson, A. *Phys. Rev. Lett.* **1998**, *81* (8), 1730.
- (53) Freund, H. J. *J. Am. Chem. Soc.* **2016**, *138*, 8985.